Time-Variant Pilot- and CP-Aided Channel Estimation for GFDM

Shahab Ehsanfar*, Marwa Chafii**, *IEEE Member*, Gerhard Fettweis*, *IEEE Fellow*

*Vodafone Chair Mobile Communications Systems, Technische Universität Dresden, Germany
**ETIS UMR 8051, Université Paris-Seine, Université de Cergy-Pontoise, ENSEA, CNRS, France
{*shahab.ehsanfar, fettweis*}*@ifn.et.tu-dresden.de*, *marwa.chafii@ensea.fr*

***Abstract*—We consider the channel estimation (CE) of a non-orthogonal multi-carrier system where the wireless channel is both frequency-selective and time-variant. In non-orthogonal multi-carriers e.g. generalized frequency division multiplexing (GFDM), the reference signals for channel estimation become contaminated by the data symbols, which consequently, limits the transceiver performance. On the other hand, the well time-localization of the pilot symbols in GFDM, allows a more efficient use of cyclic prefix (CP). Particularly, by localizing the energy of the pilot symbols to the end of block, it is possible to use the pilot's information also from CP for channel estimation. Moreover, since in a non-orthogonal waveform, the energy concentration of the pilots might not be uniform over the transmit block duration, the CE algorithm that relies solely on block-fading assumptions might have its best performance at a specific time sample within the block duration. The knowledge of such time sample is specifically important for deriving the channel autocorrelation for adaptive filtering in time-variant situations. In this paper, we first propose an approach to efficiently use the whole transmission block for channel estimation including its CP, and then, we derive the well-known adaptive Wiener-Hopf filters for CE of the non-orthogonal interference-limited GDFM system. From the simulation results, we observe that using CP information for channel estimation and applying the Wiener-Hopf filters achieves up to 1.45 dB smaller frame error rate in comparison to an orthogonal frequency division multiplexing system.**

I. Introduction

Vehicle-to-Vehicle and Vehicle-to-Infrastructure communication is currently playing a key role for the fifth generation (5G) wireless networks and beyond. A major challenge of the vehicular wireless communication is the time-varying transfer function of the wireless channel. In urban and suburban scenarios, due to the mobility of the transceivers and also due to the reflections from surrounding objects, the wireless channel for broadband type of communications becomes doubly dispersive. Orthogonal frequency division multiplexing (OFDM) that has been selected for early releases of 5G standardization [1] loses its orthogonality between subcarriers, if the channel subjects to frequency dispersion. Non-orthogonal multi-carriers e.g. generalized frequency division multiplexing (GFDM) [2] partially abandon the strict orthogonality principle, while they emphasis on better controlling the impairments of the waveform. For instance, it has been shown [3] that the flexibility of GFDM covers a wide range of application types from enhanced mobile broadband (eMBB) to ultra reliable low latency communication (URLLC) to internet of things (IoT), although, it also represents a trade-off between complexity and performance.

A common drawback of most OFDM-variant waveforms is transmission of each symbol on a single frequency bin. Should the corresponding frequency bin subject to deep fading, the information in such symbol is completely lost. This necessitates the OFDM waveform to adopt a strong enough bit-interleaved-code to cope with the situation. However, in non-orthogonal waveforms such as GFDM due to spreading multiple symbols on multiple frequency bins, it is possible to gain further diversity and thus, improve the robustness of transmission. For instance, it has been shown in [4] and [5] that GFDM can exploit the frequency diversity and achieve an improved detection performance leading to higher capacity bound [6] compared to OFDM. Furthermore, the well time-localization of the pilots in GFDM allows to reuse the energy of the pilots from cyclic prefix (CP).

The idea to use the CP information for OFDM channel estimation was explored in [7] and [8] via Kalman filters, though, their approach is limited only to orthogonal waveforms. In this work, we take advantage of symbol-time-localization in GFDM in order to improve the channel estimation (CE) performance by reusing the pilots' information from CP. In other words, if we properly allocate the pilots in time domain such that their most energy is localized at the end of the block, they would have also a high energy when copied into the CP. Unlike [7] and [8], this work proposes an approach for any linear modulation where the receiver might be inter-symbol- (ISI) and/or inter-carrier-interference (ICI) limited. To the best of our knowledge no similar results on time-variant non-orthogonal channel estimation have been published in literature that takes advantage of pilots' information from CP.

Our main contributions in this paper follow:

a. We build upon our prior works on pilot-aided GFDM CE [9] and [10] by proposing a new technique to reuse the pilots' information from the CP. In non-orthogonal multi-carriers, pilots are contaminated with the data symbols transmitted on the same subcarrier. The pilot contamination from the data symbols is not easily removable because the interference statistics are correlated with the channel statistics. Therefore, in order to derive the LMMSE channel estimator with a tractable manner of calculating interference statistics, we propose

an approach to simplify the non-diagonalizable equivalent channel. Further details of this approach in multiple-input-multiple-output applications are reported in our recent work [11].

b. Considering transmission of multiple GFDM blocks[1] in time-variant scenarios, we derive and apply the well-known Wiener-Hopf filters [12] to the non-orthogonal interference-limited received signal. Through, extensive simulations, we examine the performance of pilot- and CP-aided GFDM CE and we compare it to the performance of OFDM signal.

Notations

Column-vectors are denoted by vector sign $\vec{X}$ and matrices by boldface $\mathbf{X}$. $\mathbb{E}[\cdot]$ is the expectation operator. The transpose and Hermitian transpose of $\boldsymbol{X}$ are denoted by $\boldsymbol{X}^T$ and $\boldsymbol{X}^H$, respectively. $\boldsymbol{X} \oplus \boldsymbol{Y}$ and $\boldsymbol{X} \circ \boldsymbol{Y}$ are the direct sum and Hadamard product [13] of matrices $\boldsymbol{X}$ and $\boldsymbol{Y}$, respectively. $\mathrm{diag}(\vec{X})$ is a diagonal matrix whose diagonal entries are the entries of the column vector $\vec{X}$. $\mathtt{vec}(\boldsymbol{X})$ is the operation of stacking the columns of $\boldsymbol{X}$ on top of one another. The matrices $\boldsymbol{F}_n$ and $\boldsymbol{I}_n$ are the unitary DFT and the identity matrices of size $n \times n$, respectively. The matrix $\mathbf{0}_{m\times n}$ is an all *zero* matrix of size $m \times n$. $\vec{0}_n$ is an all *zero* column vector of size n. The distribution of a circularly symmetric complex Gaussian random vector $\vec{X}$ with mean $\vec{\mu} = \mathbb{E}[\vec{X}]$ and covariance matrix $\boldsymbol{\Sigma} = \mathbb{E}[(\vec{X} - \vec{\mu})(\vec{X} - \mu)^H]$ is denoted by $\mathcal{N}_C(\vec{\mu}, \boldsymbol{\Sigma})$.

II. System Model

A. Transmit Signal

Consider digital baseband signal $\vec{x}_b \in \mathbb{C}^N$ associated to GFDM block $b \in \{1, \cdots, B\}$ and linearly modulated by a modulation matrix $\boldsymbol{\mathcal{M}} \in \mathbb{C}^{N\times N}$, i.e.

$$\vec{x}_b = \boldsymbol{\mathcal{M}}\vec{d}_b, \tag{1}$$

where $\vec{d}_b \in \mathbb{C}^N$ is a sequence of complex values decomposed into $\vec{d}_b = \vec{d}_{b,d} + \vec{d}_{b,p}$. The vector $\vec{d}_{b,d}$ carries the encoded information bits associated to block b and being mapped into complex constellation diagram (e.g. 2^μ-QAM), while $\vec{d}_{b,p}$ contains the reference symbols (i.e. *pilots*). We further assume that $\vec{d}_d \circ \vec{d}_p = 0$ which implies that the data and pilot symbols are not superimposed, but multiplexed. In case of orthogonal modulation as in OFDM, $\boldsymbol{\mathcal{M}}$ would be defined by discrete Fourier transform (DFT) matrix, i.e. $\boldsymbol{\mathcal{M}}_{\mathrm{OFDM}} = \boldsymbol{F}^H$. In non-orthogonal systems, $\boldsymbol{\mathcal{M}}$ performs any linear operation not limited to $\boldsymbol{F}^H$. For instance, in GFDM, the individual subcarriers are pulse shaped by a prototype filter circularly shifted in time and/or in frequency. Formally, we define the GFDM modulation matrix $\boldsymbol{\mathcal{M}}_{\mathrm{GFDM}} = \boldsymbol{A}$ [14] as

$$\boldsymbol{A} \triangleq \left(\vec{g}_{0,0}, \cdots, \vec{g}_{K-1,0}, \vec{g}_{0,1}, \vec{g}_{1,1}, \cdots, \vec{g}_{K-1,M-1}\right), \tag{2}$$

where $\vec{g}_{k,m} = \left(g_{k,m}[n]\right)^T_{n=0,1,\cdots,N-1}$ with $N = MK$ is the prototype filter at subcarrier index k and subsymbol index m. Moreover, the vector $\vec{d}_{b,\mathrm{GFDM}} = \mathtt{vec}(\mathbf{D}_b)$, where

[1]A block refers to a set of modulated symbols which are protected by CP.

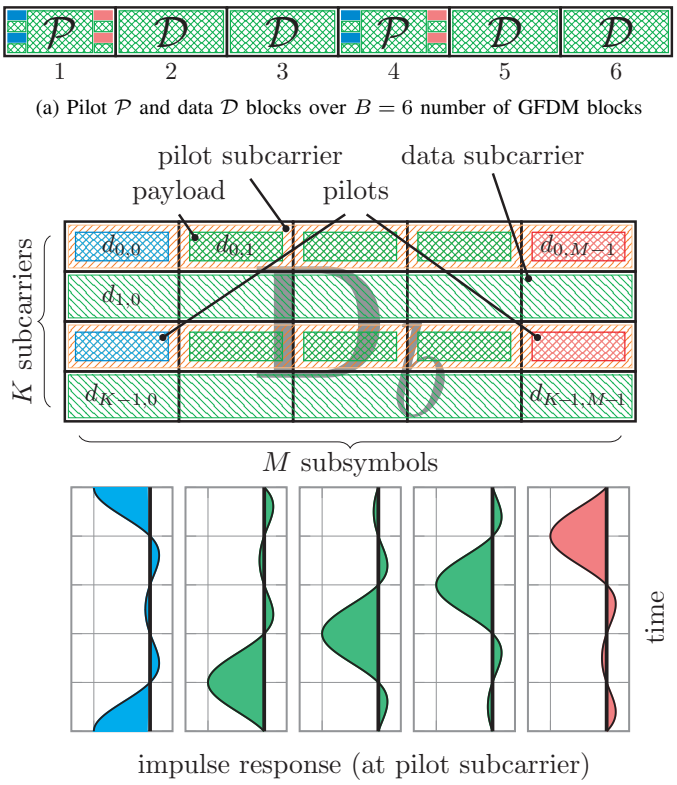

(a) Pilot $\mathcal{P}$ and data $\mathcal{D}$ blocks over $B = 6$ number of GFDM blocks

(b) Pilot insertion into the $\mathbf{D}_b$ matrix of $\mathcal{P}$-type blocks and their corresponding impulse responses

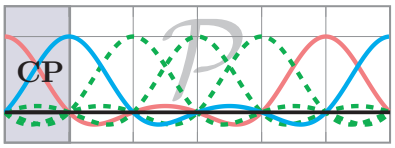

(c) Impulse response of the pilots and their energy inside CP (dashed green lines are payload pulses)

Fig. 1. Example of pilots pattern for GFDM transmission

$\mathbf{D}_b \in \mathbb{C}^{K\times M}$ is the allocation matrix for K subcarriers and M subsymbols at block b.

1) Pilot insertion: We adopt rectangular grid type of pilot pattern from [10] for every Δb GFDM block, i.e. one pilot into the first and one pilot into the last subsymbol of every Δk subcarrier. Fig. 1 illustrates an example of the pilot allocation over $B = 6$ blocks. According to Fig. 1a, the channel should be estimated at $\mathcal{P}$-type GFDM blocks, i.e. $b = \{1, 4\}$, while at the $\mathcal{D}$-type blocks it must be either interpolated, i.e. for $b = \{2, 3\}$, or be predicted, i.e. for $b = \{5, 6\}$. Note that at $\mathcal{P}$-type GFDM blocks, scattered pilots (blue and red) are multiplexed with payloads (green) as depicted in Fig. 1b, whereas the $\mathcal{D}$-type GFDM blocks carry only payloads with $\vec{d}_{b,p} = \vec{0}_N$. Furthermore, from the impulse responses shown in Fig. 1b, one may notice that the two pilots possess considerable energy at the end of the block. Hence, setting the CP duration to $N_{\mathrm{CP}} = K$ samples, would also lead to high pilots' energy from CP, when the last N_{CP} samples are copied to the beginning of the block, i.e. Fig 1c.

B. Wireless Channel

We assume a multipath Rayleigh fading channel with $L < N_{\mathrm{CP}}$ non-zero taps. The channel impulse response (CIR) is modeled as a linear finite-impulse-response filter given by

$$h[n] = \sum_{\ell=0}^{L-1} h_\ell \delta\left[n - \tilde{n}_\ell\right], \tag{3}$$

where $\tilde{n}_\ell$ is the delay of the ℓ-th tap. h_ℓ is the envelope of the CIR at tap ℓ and it can be written as a complex value with its *real* and *imaginary* components independent and identically distributed (i.i.d.) zero mean Gaussian processes parametrized by the profile $\mathbb{E}[|h_\ell|^2] = P[\ell]$. In vector notations, we write the CIR at sample realization n as

$$\vec{h}_n = \sqrt{\mathrm{diag}(\vec{P})}\vec{\mathfrak{g}}_n, \tag{4}$$

where $\vec{\mathfrak{g}}_n \sim \mathcal{N}_C(\vec{0}, \boldsymbol{I}_L)$, and $\vec{P} \in \mathbb{R}^L$ is the normalized power-delay-profile (PDP). In frequency domain, the channel response becomes

$$\vec{H}_n = \boldsymbol{F}_{N,L}\vec{h}_n, \tag{5}$$

therein, $\boldsymbol{F}_{N,L} \subseteq \boldsymbol{F}_N$ denotes the first L columns of the N-point DFT matrix.

Under the assumption of perfect time and frequency synchronization, the received signal $\vec{y}_b$ associated to block b becomes

$$\vec{y}_b = \boldsymbol{\mathcal{C}}_N\vec{x}_b + \vec{w}_b, \tag{6}$$

where $\vec{w}_b \in \mathbb{C}^N$ is the vector of additive white Gaussian noise (AWGN) samples. $\boldsymbol{\mathcal{C}}_N \in \mathbb{C}^{N\times N}$ is the matrix of CIRs with $\vec{h}$ at the beginning of its first column. In a block-fading scenario, the CIR $\vec{h}_n$ remains constant on every column of $\boldsymbol{\mathcal{C}}_N$ (i.e. $\vec{h}_n = \vec{h}_{n'}$), and therefore, $\boldsymbol{\mathcal{C}}_N$ becomes a circulant matrix (due to the CP insertion). In a time-variant situation, every tap of $\vec{h}_n$ varies with n depending on a normalized Doppler frequency given by $\nu_D = f_d/F_b$, where f_d denotes the maximum Doppler shift and F_b denotes the block rate in Hertz (Hz). The temporal correlation of the elements of $\vec{h}_n$ with their corresponding taps on $\vec{h}_{n'}$ becomes

$$r_{n,n'} = \mathbb{E}(h_n[\ell]^* h_{n'}[\ell]), \tag{7}$$

which consequently, follows with the channel autocorrelation matrix

$$[\mathbf{R}'_h]_{n,n'} = r_{n,n'} \text{ for } n, n' \in \{0, \cdots, BN' - 1\}. \tag{8}$$

III. CP-Aided Channel Estimation

In this section we propose an approach on how to simplify the equivalent channel and use the whole $\mathcal{P}$-type GFDM block including its CP for channel estimation.

In order to take into account the ISI that leaks from a $\mathcal{D}$-type GFDM block into the $\mathcal{P}$-type block, assume the channel is block fading over $N'' = 2N_{\mathrm{CP}}+N$ samples, i.e. N_{CP} samples of a block prior to $\mathcal{P}$-type GFDM block and $N' = N_{\mathrm{CP}} + N$ samples of the $\mathcal{P}$-type block. Thus, the received (Rx) signal follows:

$$\vec{y}_{b,N''} = \boldsymbol{\mathcal{T}}_{N''}\vec{x}_{b,N''} + \vec{w}_{b,N''}, \tag{9}$$

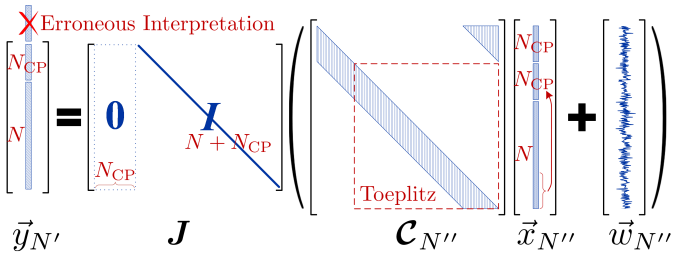

Fig. 2. Matrix structures in the modified system model (14)

where $\boldsymbol{\mathcal{T}}_{N''} \in \mathbb{C}^{N''\times N''}$ is the Toeplitz channel matrix with $\vec{h}_n$ on its first column, and $\vec{w}_{b,N''} \in C^{N''}$ being the vector of AWGN samples. $\vec{x}_{b,N''}$ contains N_{CP} samples of $\vec{x}_{b-1}$ and N' samples of $\vec{x}_b$ and its CP. Formally, we express $\vec{x}_{b,N''}$ as

$$\begin{aligned}\vec{x}_{b,N''} &= \vec{x}_{b,p,N''} + \vec{x}_{b,d,N''} \\ &= \boldsymbol{\mathcal{M}}_{N''}([\vec{0}_N^T\ \vec{d}_{b,p}^T]^T + [\vec{d}_{b-1,d}^T\ \vec{d}_{b,d}^T]^T),\end{aligned} \tag{10}$$

where the matrix $\boldsymbol{\mathcal{M}}_{N''}$ is defined as

$$\boldsymbol{\mathcal{M}}_{N''} \triangleq \left(\boldsymbol{\mathcal{M}}_{\mathrm{CP}} \oplus [\boldsymbol{\mathcal{M}}_{\mathrm{CP}}^T\ \boldsymbol{\mathcal{M}}^T]^T\right) \in \mathbb{C}^{N''\times 2N}. \tag{11}$$

Here, $\boldsymbol{\mathcal{M}}_{\mathrm{CP}}$ is the last N_{CP} columns of $\boldsymbol{\mathcal{M}}$.

In order to focus on parts of $\vec{y}_{b,N''}$ where pilots have energy, define the windowing matrix $\boldsymbol{J} \in \mathbb{R}^{N'\times N''}$ as

$$\boldsymbol{J} \triangleq [\mathbf{0}_{N'\times N_{\mathrm{CP}}}\ \boldsymbol{I}_{N'}]. \tag{12}$$

Thus, the observed signal of interest follows:

$$\vec{y}_{b,N'} = \boldsymbol{J}\vec{y}_{b,N''} = \boldsymbol{J}(\boldsymbol{\mathcal{T}}_{N''}\vec{x}_{b,N''} + \vec{w}_{b,N''}). \tag{13}$$

The linear model (13) contains a defective channel matrix $\boldsymbol{\mathcal{T}}_{N''}$, which is not unitary diagonalizable. If $\boldsymbol{\mathcal{T}}_{N''}$ were to be unitary-diagonalizable, it had to be a normal matrix. However, a matrix is simultaneously triangular and normal if and only if it is diagonal, which is not true for a multi-tap channel matrix $\boldsymbol{\mathcal{T}}_{N''}$. If $\boldsymbol{\mathcal{T}}_{N''}$ could be diagonalized, not only the complexity could be reduced, but also the theoretical calculations of the interference statistics could be done in a tractable and straightforward fashion. Thus, in order to overcome with the defectiveness of $\boldsymbol{\mathcal{T}}_{N''}$, we treat the channel matrix as circulant, despite the fact that such treatment would lead to erroneous interpretation. Therefore, we redefine the observed signal as [11]

$$\vec{y}_{b,N'} \triangleq \boldsymbol{J}(\boldsymbol{\mathcal{C}}_{N''}\vec{x}_{b,N''} + \vec{w}_{b,N''}), \tag{14}$$

where $\boldsymbol{\mathcal{C}}_{N''} \in \mathbb{C}^{N''\times N''}$ is a circulant matrix with respect to $\vec{h}$. Note that in (14), the matrix $\boldsymbol{\mathcal{C}}_{N''}$ is not the actual channel matrix, but a unitary-diagonalizable matrix, which allows to model the actual Toeplitz channel matrix of size N' (as depicted in Fig. 2). In fact, treating $\boldsymbol{\mathcal{T}}_{N''}$ as $\boldsymbol{\mathcal{C}}_{N''}$ would cause erroneous interpretation to the first N_{CP} samples of $\vec{y}_{b,N''}$. But since the windowing matrix $\boldsymbol{J}$ selects the last N' samples of $\vec{y}_{b,N''}$ and discards the first N_{CP} samples, such erroneous interpretation is pulled out, and the observation $\vec{y}_{b,N'}$ would be identical to the last N' samples of $\vec{y}_{b,N''}$.

The new model (14) provides the benefit to diagonalize the channel matrix. Thus, we have:

$$\vec{y}_{b,N'} = \boldsymbol{J}\left(\boldsymbol{F}_{N''}^{H}\mathrm{diag}(\vec{H}_{N''})\boldsymbol{F}_{N''}\vec{x}_{b,N''} + \vec{w}_{b,N''}\right), \quad (15)$$

with $\vec{H}_{N''} = \sqrt{N''}\boldsymbol{F}_{N'',L}\vec{h}$. Since we aim to estimate the parameters vector $\vec{h}$, we reorder (15) as

$$\vec{y}_{b,N'} = \boldsymbol{J}\left(\sqrt{N''}\boldsymbol{F}_{N''}^{H}\boldsymbol{X}_{b,N''}\boldsymbol{F}_{N'',L}\vec{h} + \vec{w}_{b,N''}\right), \quad (16)$$

where $\boldsymbol{X}_{b,N''} = \mathrm{diag}(\boldsymbol{F}_{N''}\vec{x}_{b,N''})$. Defining the matrix $\boldsymbol{Q} \in \mathbb{C}^{N'\times L}$ as

$$\boldsymbol{Q} \triangleq \sqrt{N''}\boldsymbol{J}\boldsymbol{F}_{N''}^{H}\boldsymbol{X}_{b,N''}\boldsymbol{F}_{N'',L}, \quad (17)$$

we obtain a general linear model in which, we can calculate the LMMSE estimate of $\vec{h}$ via Bayesian Gauss-Markov theorem [12]. Thus,

$$\hat{\vec{h}}_{b,\mathrm{CPLMMSE}} = \boldsymbol{\Sigma}_{hh}\boldsymbol{Q}_p^{H}(\boldsymbol{Q}_p\boldsymbol{\Sigma}_{hh}\boldsymbol{Q}_p^{H} + \boldsymbol{\Sigma}_{\Psi\Psi}^{\boldsymbol{J}})^{-1}\vec{y}_{b,N'}, \quad (18)$$

$$\widehat{\boldsymbol{\Sigma}}_{hh} = \boldsymbol{\Sigma}_{hh} - \boldsymbol{\Sigma}_{hh}\boldsymbol{Q}_p^{H}(\boldsymbol{Q}_p\boldsymbol{\Sigma}_{hh}\boldsymbol{Q}_p^{H} + \boldsymbol{\Sigma}_{\Psi\Psi}^{\boldsymbol{J}})^{-1}\boldsymbol{Q}_p\boldsymbol{\Sigma}_{hh}, \quad (19)$$

where $\boldsymbol{Q}_p = \sqrt{N''}\boldsymbol{J}\boldsymbol{F}_{N''}^{H}\mathrm{diag}(\boldsymbol{F}_{N''}\vec{x}_{b,p,N''})\boldsymbol{F}_{N'',L}$ is the observation matrix with respect to the pilots signal $\vec{x}_{b,p,N''}$ defined in (10). Here, we omit the subscript index b for $\boldsymbol{Q}_p$ by assuming that all $\mathcal{P}$-type blocks transmit identical pilots signal $\vec{x}_{b,p,N''}$. The matrix $\boldsymbol{\Sigma}_{\Psi\Psi}^{\boldsymbol{J}} \in \mathbb{C}^{N'\times N'}$ is the covariance of noise plus interference term with respect to data signal $\vec{x}_{d,N''}$ as well as noise vector $\boldsymbol{J}\vec{w}_{b,N''}$. We calculate $\boldsymbol{\Sigma}_{\Psi\Psi}^{\boldsymbol{J}}$ in analogous way as in [10] while we also take into account the additional matrices $\boldsymbol{J}\boldsymbol{F}_{N''}^{H}$ at the left hand side of the observed signal.

IV. Adaptive filtering based on Wiener-Hopf approach

In transmission of B blocks with Rx signal model (6), the channel not only varies from one block to another, but also within each block. If the frequency-dispersion of the channel is considerable, i.e. $\nu_D > 1\%$, equalizing the $\mathcal{D}$-type blocks with the channel estimations at $\mathcal{P}$-type blocks is not thoughtful. In fact, the channel has to be interpolated for the data blocks between two $\mathcal{P}$-type blocks and be predicted for those which follow the last pilot-scattered block. Furthermore, given multiple channel estimations at different $\mathcal{P}$-type blocks, such estimations can be further improved.

Define the auto-correlation matrix $\mathbf{R}_h \in \mathbb{C}^{B\times B}$ being a sub-matrix of $\mathbf{R}'_h$ with each of its rows/columns being the $n_{p,b}$-th row/column of $\mathbf{R}'_h$. $n_{p,b}$ denotes a sample index within the duration of block b, in which, the channel estimation is expected to have its best performance and it is obtained via

$$n_{p,b} = (b-1)N' + N_0 + \frac{\sum_{n=1}^{N_{x_p}} nP_{x_p}[n]}{\sum_{n=1}^{N_{x_p}} P_{x_p}[n]}, \quad (20)$$

which is the weighted average of the sample indexes with the pilot's power $P_{x_p}[n]$ as the weighting coefficient. N_0 denotes the number of initial samples that are not used for CE, N_{x_p} denotes the length of pilots' signal that is used for CE e.g. If the whole block including its CP is used for CE, we have $N_{x_{p,N'}} = N', N_0 = 0$ and $\vec{P}_{x_{p,N'}} = |\vec{x}_{b,p,N'}|^2$, whereas for a CE with CP-less pilots' signal, we have $N_{x_{p,N}} = N, N_0 = N_{\mathrm{CP}}$ and $\vec{P}_{x_{p,N}} = |\vec{x}_{b,p,N}|^2$. $\vec{x}_{b,p,N'}$ and $\vec{x}_{b,p,N}$ denote the last N' and the last N elements of $\vec{x}_{b,p,N''}$, respectively. The above choice of $n_{p,b}$ will be further justified in Sec. V.

The joint *smoothing-interpolation-prediction* of the channel at ℓ-th tap and b-th block based on Wiener-Hopf approach [12] follows:

$$\hat{h}_{\ell,b} = [\vec{R}_h]_{\mathcal{P},b}^{H}(\mathbf{R}_h^{(\mathcal{P})} + \hat{\sigma}_\ell^2\boldsymbol{I}_{B_p})^{-1}\hat{\vec{h}}_\ell, \quad (21)$$

where $[\vec{R}_h]_{\mathcal{P},b} \subset \mathbf{R}_h$ is the b-th column of $\mathbf{R}_h$ with row indexes corresponding to $\mathcal{P}$-type block indexes. The sub-matrix $\mathbf{R}_h^{(\mathcal{P})} \subseteq \mathbf{R}_h$ contains the rows and columns of $\mathbf{R}_h$ associated to $\mathcal{P}$-type blocks. $\hat{\sigma}_\ell^2$ denotes the ℓ-th diagonal element of $\widehat{\boldsymbol{\Sigma}}_{hh}$. B_p denotes the number of pilot blocks. $\hat{\vec{h}}_\ell \in \mathbb{C}^{B_p}$ is the vector of channel estimations at tap ℓ and at $\mathcal{P}$-type blocks. Note that the channel estimation in (18) is L-dimensional and corresponds to the sample time index $n_{p,b}$, whereas $\hat{\vec{h}}_\ell$ contains the ℓ-th element of $\hat{\vec{h}}_{b,\mathrm{CPLMMSE}}$ defined in (18) for multiple estimations at $\mathcal{P}$-type blocks.

V. Simulation Results

In this section, we examine the performance of the proposed CP-aided CE and the adaptive filtering for time varying channels via Monte-Carlo simulations. Consider a Rayleigh fading multipath channel with exponential PDP where, $P_\ell = [10^{P_\ell^{\mathrm{dB}}/10}]_{\ell=0,\cdots,L-1}^{T}$ and P_ℓ^{dB} decreases linearly from 0 to -20 dB. We consider $L = 9$ taps of the channel which corresponds to 4.7μs length of impulse response for sampling frequency of 1.92 MHz. Each tap of the impulse response $\vec{h}[n]$ is temporally correlated according to [15] $r_{n,n'} = J_0(2\pi(n-n')\nu_D)$, where $J_0(\cdot)$ is the zeroth order Bessel function of the first kind. The transmit information bits are encoded through *Parallel Concatenated Convolutional Codes* with octal generator polynomial (1, 15/13) and code-rate r. The number of transmission blocks is set to $B = 15$, and from $b = 1$, every $\Delta b = 3$-rd block, we multiplex pilots with the data symbols. For GFDM, we consider blocks $M = 7$ subsymbols are transmitted over $K = 48$ subcarriers. Pilots in form of first root Zadoff-Chu sequence are inserted according to Fig. 1 with pilot subcarrier spacing $\Delta k = 2$. The above GFDM configuration yields 4.76% pilots overhead. Raised-Cosine (RC) with roll-off factor 0.3 has been chosen as the GFDM prototype filter. As a comparison benchmark, we adopt $B_{\mathrm{OFDM}} = 15$ OFDM symbols over $K_{\mathrm{OFDM}} = MK$ subcarriers while one OFDM symbol has the same time duration of a GFDM block. Hence, with the assumption of having identical bandwidth for both systems, the subcarriers for GFDM become M times broader than the OFDM subcarriers. In order to maintain the same pilot overhead also for OFDM, we set $\Delta k_{\mathrm{OFDM}} = 2M$ and $\Delta b_{\mathrm{OFDM}} = 3$. The signal-to-noise ratio (SNR) is denoted by $\mathcal{E}_s/N_0$ and adding the gain of modulation and coding we have $\mathcal{E}_b/N_0 = \mathcal{E}_s/N_0 - 10\log_{10}\mu r$, where μ is the modulation-order. The receivers for both systems

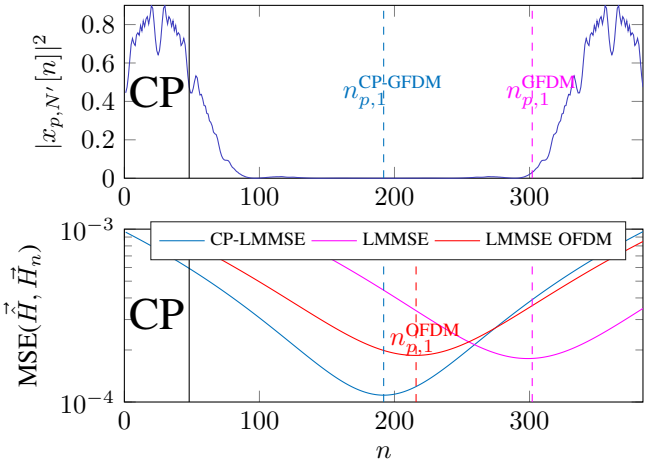

Fig. 3. Mean Squared Error of the channel within one block duration. Dashed lines are the theoretical values of $n_{p,b}$ defined in (20).

adopt Component-Wise Conditionally Unbiased LMMSE estimation [5, Sec. II.B] for joint equalization of the wireless channel and the GFDM/OFDM matrix $\boldsymbol{\mathcal{M}}$. Thereupon, the equalized signal constellations are transformed into *maximum likelihood* (ML) log-likelihoods and they are then softly decoded with 8 turbo iterations.

Fig. 3 illustrates an example of pilots signal in time domain, i.e. $\vec{x}_{p,N'} = [\boldsymbol{\mathcal{M}}_{\text{CP}}^T \ \boldsymbol{\mathcal{M}}^T]^T \vec{d}_{b,p}$ (the upper figure), and the mean squared error (MSE) of the CE $\hat{\vec{H}} = \boldsymbol{F}_{N,L} \hat{\vec{h}}_b$ with respect to each channel realization $\vec{H}_n$ at sample time instant n and $\mathcal{E}_s/N_0 = 30$ dB (the lower figure). One can see that the minimum error of the channel estimation—with block-fading assumption—within the block duration happens at the weighted average of the pilot signal $n_{p,1}^{\text{CP-GFDM}}$ (with CP) and $n_{p,1}^{\text{GFDM}}$ (without CP). For OFDM, the minimum error happens at the center of the N-length CP-less signal because the pilots in OFDM have uniform energy over the whole duration of N samples. Fig. 3 confirms the choice of $n_{p,b}$ in (20) for defining the autocorrelation matrix $\mathbf{R}_h$ out of $\mathbf{R}'_h$ because the CE has its best performance at sample instance $n_{p,b}$.

Fig. 4 compares the performance of channel estimation in terms of MSE for GFDM LMMSE and CP-LMMSE estimations as well as OFDM CP-LMMSE. We consider two time-variant channel scenarios with $f_d = 70$ Hz and $f_d = 300$ Hz. The corresponding normalized Doppler frequency for each scenario becomes $\nu_D = 1.23\%$ and $\nu_D = 5.25\%$, respectively. In addition, the block-fading assumption calculates the MSE of the estimated channel at $\mathcal{P}$-type blocks with respect to the channel realizations within the duration of $\mathcal{P}$-type block itself and also its following two $\mathcal{D}$-type blocks. The Wiener filtering performs channel smoothing at $\mathcal{P}$-type blocks $b^{(\mathcal{P})} = \{1, 4, 7, 10, 13\}$, channel interpolation at $\mathcal{D}$-type blocks $b^{(\mathcal{D})} = \{2, 3, 5, 6, 8, 9, 11, 12\}$ and channel prediction at the last two $\mathcal{D}$-type blocks $b^{(\mathcal{D})} = \{14, 15\}$. From Fig. 4a and Fig. 4b, it can be observed that the optimum CE performance is achieved via GFDM's CP-LMMSE with Wiener filter, which is due to the fact that the total pilot's energy including the CP in GFDM becomes larger than the one in OFDM as well as CP-less GFDM. Although, at very high SNR regions in Fig. 4a, OFDM becomes slightly better than GFDM's CP-LMMSE because of the self interference from data symbols in GFDM. Such behavior does not happen in Fig. 4b because the error floor due to the self-interference in GFDM is at a much lower lever compared to the error floor due to the channel variations in OFDM. We also note that using the proposed CP-LMMSE approach does not considerably improve the CE performance in OFDM because the pilot's energy is uniformly distributed over the whole symbol duration and thus an OFDM system lacks of an efficient pilot time-localization. Comparing the simulation curves with block-fading assumption, we observe that at very low SNR regions, CP-LMMSE has smaller MSE with respect to OFDM and CP-less GFDM, while at high SNR regions the error floor due to the channel variations becomes significant for three approaches.

The transceiver performance for two modulation and coding scheme (MCS) of QPSK 1/3 and 16-QAM 2/3 is provided in Fig. 5. Since in channel estimation MSE results, we observed that the approaches with Wiener filtering has outperformed the results with block-fading assumptions, here we compare the performance for Wiener filter approaches. As can be expected from the CE MSE results, GFDM's CP-LMMSE outperforms OFDM and CP-less GFDM in terms of frame error rate (FER) for both MCS as well as both time-variant scenarios of $f_d = 70$ Hz and $f_d = 300$ Hz. Although, the performance improvement is almost negligible for a robust MCS of QPSK 1/3, the SNR gap becomes much larger up to 1.45 dB for a target FER of 10^{-1} in 16-QAM 2/3 and $f_d = 300$ Hz, i.e. Fig. 5b. Comparing the CP-less GFDM's LMMSE with OFDM, we observe that albeit they almost have the same MSE performance for $\mathcal{E}_s/N_0 < 15$ dB, GFDM's LMMSE slightly outperforms OFDM in Fig. 5a, which is due to the higher frequency diversity of GFDM in frequency selective situations. In a scenario where the channel is too much time-varying i.e. Fig. 5b, OFDM outperforms GFDM's LMMSE because of its smaller error floor in CE MSE results.

VI. Conclusions

In this paper, we have proposed a new approach to improve the CE performance of GFDM by using the whole transmitted signal including its CP. Considering transmission of multiple GFDM blocks, we have also derived the adaptive Wiener-Hopf filters for joint *smoothing-interpolation-prediction* of the channel. From simulation results, we have observed that using adaptive filters for channel estimation has significantly reduced the error floor, when it is compared to the case where the CE relies solely on block-fading assumptions. We have also seen that using CP for channel estimation of GFDM, improves the transceiver performance for up to 1.45 dB compared to OFDM in a frequency-selective and time-varying situation.

Acknowledgment

The computations were performed at the Center for Information Services and High Performance Computing (ZIH)

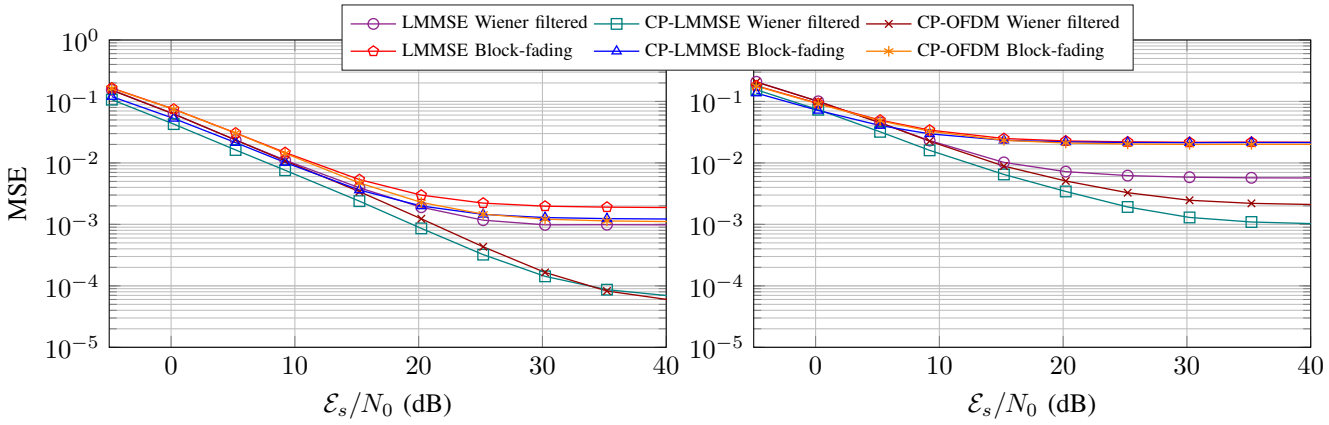

(a) $f_d = 70$ Hz (b) $f_d = 300$ Hz

Fig. 4. Time-variant channel estimation performance

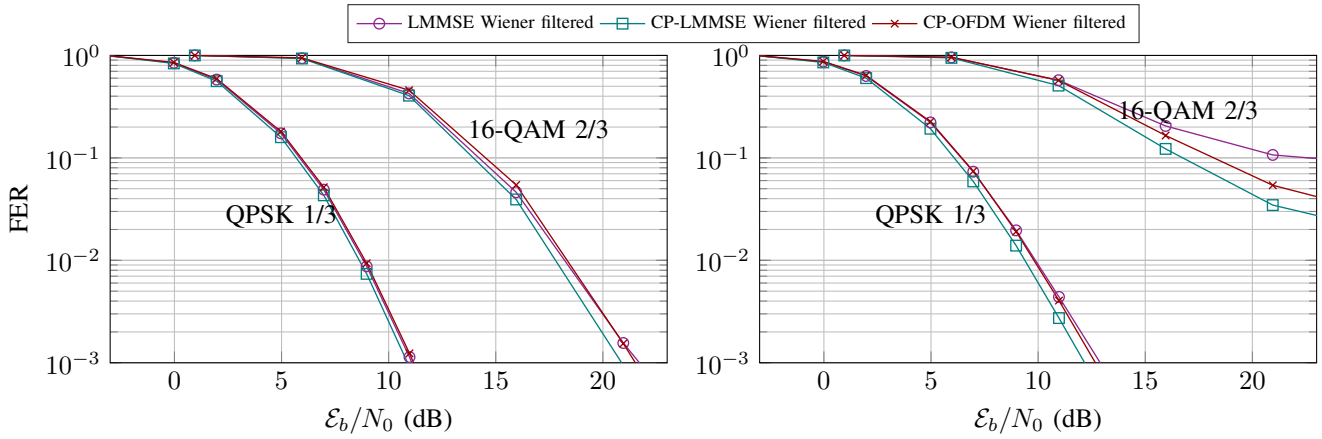

(a) $f_d = 70$ Hz (b) $f_d = 300$ Hz

Fig. 5. Frame error rate simulation results for QPSK 1/3 and 16-QAM 2/3

of TU Dresden. This work has received funding from the European Union's Horizon 2020 research and innovation program under grant agreements no. 777137 (5GRANGE project) and no. 732174 (Orca project).

REFERENCES

[1] 3GPP, "NR; NR and NG-RAN Overall Description; Stage 2, Rel. 15," 3rd Generation Partnership Project (3GPP); Tech. Spec. Group Radio Access Network, Technical Specification (TS) 38.300, 06 2018, v15.2.0.

[2] A. Nimr, S. Ehsanfar, N. Michailow, M. Danneberg, D. Zhang, H. D. Rodrigues, L. L. Mendes, and G. Fettweis, *Generalized Frequency Division Multiplexing: A Flexible Multicarrier Waveform*. Cham: Springer International Publishing, 2019, pp. 93–163.

[3] J. Ferreira, H. Rodrigues, A. Gonzalez, A. Nimr, M. Matthé, D. Zhang, L. Mendes, and G. Fettweis, "GFDM Frame Design for 5G Application Scenarios," *Journal of Communication and Information Systems*, vol. 32, no. 1, Jul. 2017.

[4] D. Zhang, L. Mendes, M. Matthé, I. Gaspar, N. Michailow, and G. Fettweis, "Expectation Propagation for Near-Optimum Detection of MIMO-GFDM Signals," *IEEE Trans. Wireless Commun.*, 2015.

[5] M. Matthé, D. Zhang, and G. Fettweis, "Low-Complexity Iterative MMSE-PIC Detection for MIMO-GFDM," *IEEE Transactions on Communications*, vol. 66, no. 4, pp. 1467–1480, April 2018.

[6] D. Zhang, M. Matthé, L. L. Mendes, and G. Fettweis, "Message passing algorithms for upper and lower bounding the coded modulation capacity in a large-scale linear system," *IEEE Signal Process. Lett.*, vol. 23, no. 4, pp. 537–540, April 2016.

[7] A. A. Quadeer and M. S. Sohail, "Enhanced channel estimation using Cyclic Prefix in MIMO STBC OFDM sytems," in *The 10th IEEE International Symp. on Signal Processing and Information Technology*, Dec 2010, pp. 277–282.

[8] A. K. Kohli and D. S. Kapoor, "Adaptive Filtering Techniques Using Cyclic Prefix in OFDM Systems for Multipath Fading Channel Prediction," *Circuits Syst. Signal Process.*, vol. 35, no. 10, pp. 3595–3618, Oct. 2016.

[9] S. Ehsanfar, M. Matthé, D. Zhang, and G. Fettweis, "A Study of Pilot-Aided Channel Estimation in MIMO-GFDM Systems," in *Proc. of the ITG/IEEE Workshop on Smart Antennas (WSA'16)*, 2016.

[10] S. Ehsanfar, M. Matthé, D. Zhang, and G. Fettweis, "Theoretical Analysis and CRLB Evaluation for Pilot-aided Channel Estimation in GFDM," in *Proc. of the IEEE Global Communications Conference (GLOBECOM'16)*, 2016.

[11] S. Ehsanfar, M. Matthé, M. Chafii, and G. Fettweis, "Pilot- and CP-Aided Channel Estimation in MIMO Non-Orthogonal Multi-Carriers," *IEEE Transactions on Wireless Communications*, vol. 18, no. 1, pp. 650–664, Jan 2019.

[12] S. M. Kay, *Fundamentals of Statistical Signal Processing: Estimation Theory*. Upper Saddle River, NJ: Prentice Hall, 1993, vol. 1.

[13] A. H. Roger and R. J. Charles, "Topics in matrix analysis," 1991.

[14] N. Michailow et. al., "Generalized Frequency Division Multiplexing for 5th Generation Cellular Networks," *IEEE Trans. Commun.*, vol. 62, no. 9, pp. 3045–3061, 2014.

[15] R. H. Clarke, "A statistical theory of mobile-radio reception," *The Bell System Technical Journal*, vol. 47, no. 6, pp. 957–1000, July 1968.